# Theory of generation of new frequencies by mixing of solitons and dispersive waves in optical fibers

D. V. Skryabin* and A. V. Yulin
*Department of Physics, University of Bath, Bath BA2 7AY, United Kingdom*
(Received 7 February 2005; published 20 July 2005)

We develop a theory of the generation of new spectral components in optical fibers pumped with a solitonic pulse and a weak continuous wave (cw). We derive the wave number matching conditions for the above process and present an analytical method of finding the amplitudes of the generated waves. We discuss related effects of the depletion of the cw pump and spectral recoil on the soliton. We also point out examples of the generation of supercontinuum spectra in fibers, where mixing between solitons and dispersive waves plays an important role.

DOI: 10.1103/PhysRevE.72.016619 PACS number(s): 42.81.Dp, 42.65.Ky, 42.65.Tg

## I. INTRODUCTION

A powerful laser pulse propagating inside an optical fiber and having significant part of its spectrum experiencing anomalous group velocity dispersion (GVD) usually disintegrates into a mixture of solitons and dispersive waves [1–15]. This process is fertile ground for understanding many fundamental problems in soliton physics including the interaction between solitons and the interaction of solitons with dispersive waves.

The recent rise of interest in the above problems has been fueled by availability of highly nonlinear photonic crystal and tapered fibers with core diameters of the order of and less than 1 $\mu$m [4–16]. Spectral broadening accompanying complex transformation of the femtosecond optical pulses in such fibers, usually referred to as supercontinuum generation, has attracted significant attention; see, e.g., [5–14]. Photonic crystal fibers (PCF's) have also proved to be useful for efficient conversion of light from the femtosecond solitonic pump pulse into a spectrally narrow band of the so-called Cherenkov or resonant radiation [15–17]. A peculiar mechanism leading to the exponential amplification of the resonant radiation in PCF's has also been discovered [16,17].

Until recently, the theory of Cherenkov radiation [16–22] has remained the only theory which has successfully explained some of the spectral peaks observed in highly nonlinear PCF's pumped with femtosecond pulses [11–16]. However, it has been recently shown theoretically [23] that mixing of a soliton with a weak continuous wave (cw) also leads to the generation of new spectral lines, providing that the higher-order dispersions are included into consideration. Theoretical predictions of Ref. [23] have been used to back some of the experimental measurements reported in Ref. [24]. Spectral measurements and numerical modeling reported in [25,26] have also shown that the interaction of solitons with dispersive waves leads to the generation of new spectral peaks. However, no wave number matching condition, apart from the well-known Cherenkov condition, supporting these observations has been presented in Refs. [25,26].

The aim of this work is to further develop a physical understanding and analytical methods of description of mixing between solitons and dispersive waves in optical fibers. In particular, we present further results centered around the wave number matching condition derived in Ref. [23] and develop an original technique for the calculation of the amplitudes of the waves generated via mixing of solitons and dispersive waves. We describe reactive effects of the radiation on solitons and explain how shapes of the supercontinuum spectra calculated for the experimentally viable conditions are affected by the mixing of the solitons and radiation.

## II. MODEL

We assume that dynamics of the dimensionless amplitude $A(t,z)$ of the fundamental fiber mode is governed by the generalized nonlinear Schrödinger (NLS) equation (see, e.g., [17,24]

$$\partial_z A = iD(i\partial_t)A + i|A|^2 A. \tag{1}$$

Here $t$ is dimensionless time and $z$ is the coordinate along the fiber. In what follows, the frequency dependence of $A$ is assumed in the form $e^{-i\delta t}$, where $\delta$ is the normalized frequency detuning. $D(\delta)$ is the properly shifted and normalized frequency dependence of the propagation constant of the fiber mode. All the normalizations made are detailed in Appendix A. For the purposes of the significant part of the paper it suffices to disregard the Raman effect. The role of the latter will be considered in Sec. VIII.

We assume that the fiber is pumped with a solitonic pulse and a weak—i.e., linear—continuous wave (cw), and aim to find the field generated as a result of this process. If

$$D(\delta) = -\frac{\delta^2}{2}, \tag{2}$$

then Eq. (1) is completely integrable. In this case mixing of the soliton and cw can result in shifts of the position and the

*Author to whom correspondence should be addressed. Electronic address: d.v.skryabin@bath.ac.uk; URL: http://staff.bath.ac.uk/pysdvs

 

phase of the soliton, in small oscillations of the soliton amplitude and in formation of a new eigensolution of the NLS equation in the form of the soliton nesting on the cw pedestal [27–30]. If the soliton under consideration is short and/or the slope of $\partial_\delta^2 D(\delta)$ is sufficiently steep, then the higher-order dispersions become important and the system is far from the integrable limit. In this case the most striking effect resulting from mixing of the solitons and cw's is the generation of new spectrally narrow radiation bands [23].

## III. PERTURBATION THEORY: INTRODUCTION

We look for solutions of Eq. (1) in the form

$$A = F(t)e^{iqz} + g(z,t), \quad F = \sqrt{2q}\,\mathrm{sech}(t\sqrt{2q}). \tag{3}$$

$Fe^{iqz}$ is an exact soliton solution of Eqs. (1) and (2), and $q>0$ is the shift of the soliton wave number. The $g$ term is a superposition of all the dispersive waves in the system; i.e., $g$ includes the cw pump and all the waves generated, when $D(\delta)$ deviates from Eq. (2). For our purposes below it is sufficient to include the third-order dispersion only—i.e., take $D(\delta)$ as the third-order polynomial:

$$D(\delta) = -\frac{\delta^2}{2} + \epsilon\delta^3. \tag{4}$$

Link of the parameter $\epsilon$ with physical quantities is given in Appendix A.

Assuming that $g$ is a linear wave we derive

$$i\left[D(i\partial_t) - \frac{1}{2}\partial_t^2\right]Fe^{iqz} = \partial_z g - iD(i\partial_t)g - i2F^2 g - iF^2 g^* e^{i2qz}. \tag{5}$$

Deviations of $D(i\partial_t)$ from $\frac{1}{2}\partial_t^2$ are retained not only on the left-hand side of Eq. (5), but also on its right-hand sides. This is because, even for $|\epsilon| \ll 1$, we anticipate the existence of the dispersive waves with such frequency detunings from the soliton that the third-order contribution to the overall dispersion starts to be compatible with or dominant over the second-order one; see [17] for a more detailed discussion.

We assume that $g$ consists of the two parts

$$g = we^{iD_{cw}z - i\delta_{cw}t} + \psi, \quad D_{cw} = D(\delta_{cw}). \tag{6}$$

The $w$ term in Eq. (6) is the weak cw pump, which obeys Eq. (5) when the soliton field is disregarded—i.e., $F=0$. Here $w$ is a real amplitude of the cw pump and $\delta_{cw}$ is its frequency. The $\psi$ term is the generated wave. To find the wave number matching conditions it suffices to assume that the cw pump and the soliton are the fixed sources of energy. As we will see below this assumption allows us to make excellent quantitative predictions of the frequencies of the generated waves. Substituting Eq. (6) into Eq. (5) we find

$$\begin{aligned} i\left[D(i\partial_t) - \frac{1}{2}\partial_t^2\right]Fe^{iqz} + i2F^2 we^{izD_{cw} - it\delta_{cw}} \\ + iF^2 we^{2iqz - izD_{cw} + it\delta_{cw}} \\ = \partial_z\psi - iD(i\partial_t)\psi - i2F^2\psi - iF^2\psi^* e^{2iqz}. \end{aligned} \tag{7}$$

The left-hand side of Eq. (7) consists of the three parts serving as driving for the wave $\psi$. The first part of the driving depends on the soliton field only and is proportional to the deviation of the dispersion $D(\delta)$ from the ideal parabolic form. The second and third parts originate from the mixing of the soliton and cw fields. These terms are linear in the cw amplitude and quadratic in the soliton.

## IV. WAVE NUMBER MATCHING CONDITIONS AND RESONANCE FREQUENCIES

### A. Analytics

For Eq. (7) to have the dispersive wave solutions, the operator on the right-hand side should have continuum modes, which can be excited by the left-hand side. To find these continuum modes we neglect the $F^2$ terms in the right-hand side and seek $\psi$ in the form $\psi \sim \exp(iD(\delta)z - i\delta t)$. Wave number matchning with the three driving terms in the left-hand side of Eq. (7) is achieved providing

$$q = D(\delta), \tag{8}$$

$$D_{cw} = D(\delta), \tag{9}$$

$$2q - D_{cw} = D(\delta). \tag{10}$$

Equation (8) is a well-known condition giving the frequencies of the resonance waves emitted by the soliton in the presence of the higher-order dispersions, so-called Cherenkov resonances [17–22]. Equations (9) and (10) give new resonances which depend on the cw pump [23]. These resonances are driven by the four-wave mixing (FWM) between the solitons and cw pump (see $wF^2$ terms on the left-hand side of Eq. (7)); therefore, we call them FWM resonances. All three conditions can be written as one equation

$$q + J[D_{cw} - q] = D(\delta), \quad J = -1, 0, +1. \tag{11}$$

The resonance frequencies are found by solving Eqs. (11) for $\delta$. It is clear that condition (11) involves four wave numbers: namely, $D_{cw}$ is the wave number of the cw pump, $D(\delta)$ on the right-hand side is the wave number of the generated dispersive wave, and $q$, which occurs twice, is the wave number of the Fourier harmonics of the soliton. The fact that all Fourier harmonics of the soliton have the same wave number originates from our assumption that the reference frequency $\omega_0$ (see Appendix A) coincides with the soliton central frequency. Relaxing this assumption—i.e., allowing nonzero-frequency detuning in the solitonic part of Eq. (3), as it has been done in Refs. [17,23]—makes calculations more cumbersome, but reveals that the first $q$ in Eq. (11) traces back to the wave number of the soliton at the resonance frequency, $k_{s/rad}$, and the second $q$ to the wave number of the soliton at the frequency of the cw pump, $k_{s/cw}$. Thus, in general, Eq. (11) transforms to

$$k_{s/rad} + J[\beta_{cw} - k_{s/cw}] = \beta_{rad}, \tag{12}$$

where $\beta_{cw}$ and $\beta_{rad}$ are the propagation constants of the fiber mode calculated at the frequencies of the cw pump and radiation; see Appendix A and [23].

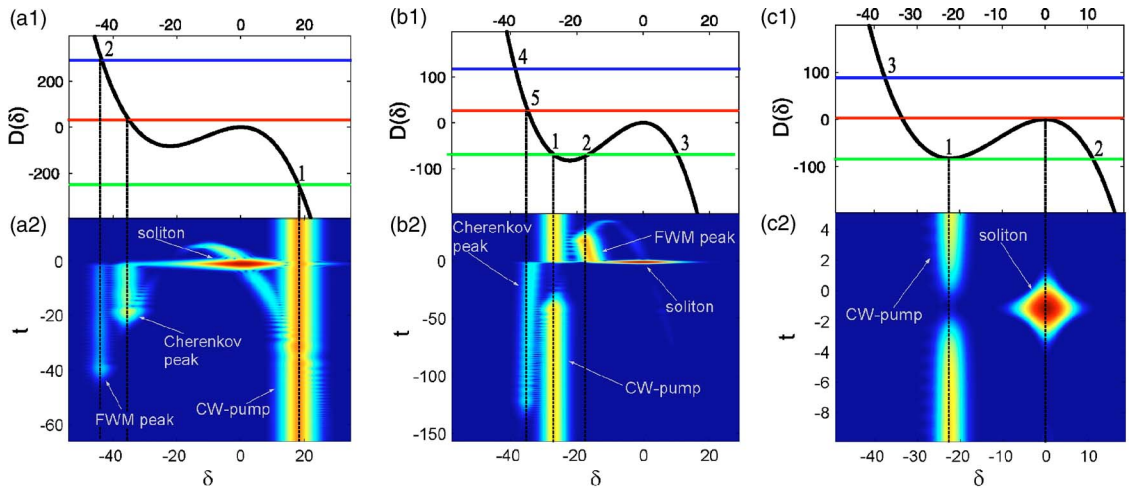


FIG. 1. (Color online) Wave number matching diagrams (top) and XFROG spectrograms (bottom), when the fiber with the negative GVD slope, $\epsilon=-0.015$, is pumped with the soliton and cw; see Eqs. (14). $w=0.4$, $a=1$, and $\delta_s=0$ in all cases. $\delta_{cw}=-18$ for (a), $-27$ for (b), and $-22.2$ for (c). Soliton parameter $q=18$ for (a),(b) and 3 for (c). Propagation distance $z$ is 1 for ($a_2$), 6 for ($b_2$), and 12 for ($c_2$).

To find the resonance frequencies we simply plot $D(\delta)$ and find when it gets equal to the left-hand sides of Eq. (11). Figures 1 ($a_1$), 1 ($b_1$), and 1 ($c_1$) show these plots for the three topologically distinct cases: ($a_1$) corresponds to the three resonances, ($b_1$) corresponds to the five resonances and ($c_1$) corresponds to the case when two resonances are degenerate. Figures 2 ($a_1$), 2 ($b_1$), and 2 ($c_1$) show the cases as in Figs. 1 ($a_1$) and 1 ($b_1$), but for the opposite sign of $\epsilon$.

It is obvious that one of the roots of Eq. (9) coincides with $\delta_{cw}$. If frequencies of the Cherenkov resonance and of the cw pump coincide—i.e., $\delta_{cw}=\delta_{ch}$, where $D(\delta_{ch})=q$—then all the three left-hand sides in Eqs. (11) become equal to $q$. Therefore, there are three degenerate resonance frequencies in this case, which coincide with $\delta_{ch}$. By deviating $\delta_{cw}$ from $\delta_{ch}$ we remove degeneracy and get three distinct resonances $\delta_{ch}+J\{\delta_{cw}-\delta_{ch}+O(|\delta_{cw}-\delta_{ch}|^2)\}$; see points 1, 4, and 5 in Fig. 1 ($b_1$). Note that the initial soliton frequency coincides with the zero of the $\delta$ axes in Figs. 1 and 2. Approximate expressions for the two resonance frequencies [see points 2 and 3 in Fig. 1 ($b_1$)] nearest to the soliton frequency, $\delta=0$, can be found assuming that $D(\delta)$ is parabolic in the proximity of the soliton. This gives the resonances at $\pm 2\sqrt{-q-j[D_{cw}-q]}+O(\epsilon)$, where $j=1$ if $D_{cw}<0$ and $j=-1$ if $D_{cw}>2q$.

### B. Modeling

In what follows it will be important for us to use a visualization tool allowing direct association of the spectral peaks with the parts of the signal in the time domain. For this we use the well-known XFROG (cross-correlation frequency-resolved optical gating) spectrograms; see, e.g., [10,13,14,24–26]. Numerically computed spectrograms in this paper are produced by plotting the integral

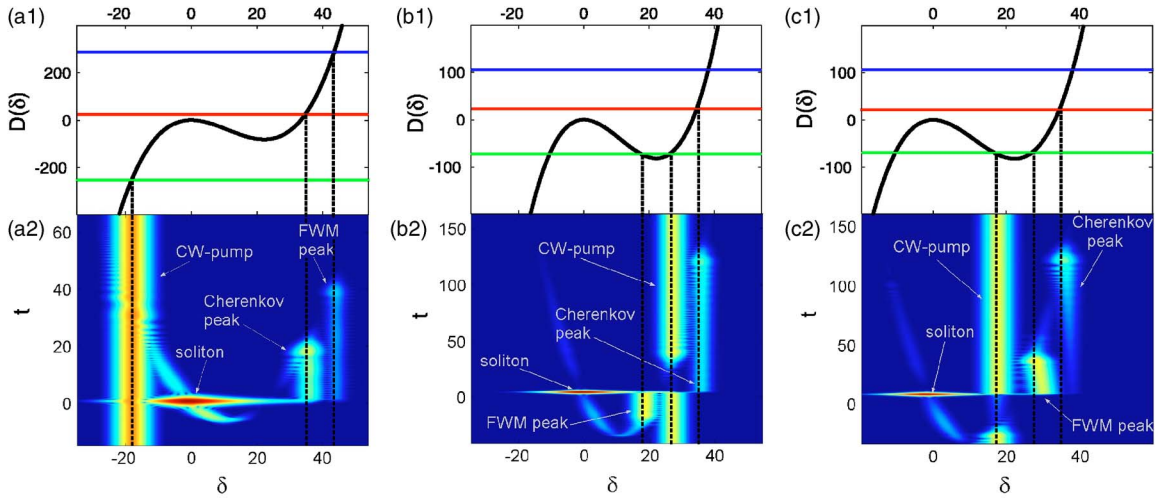


FIG. 2. (Color online) Wave number matching diagrams (top) and XFROG spectrograms (bottom), when the fiber with the positive GVD slope, $\epsilon=0.015$, is pumped with the soliton and cw; see Eqs. (14). $w=0.4$, $a=1$, $q=18$, and $\delta_s=0$ in all cases. $\delta_{cw}=-18$ for (a), 27 for (b), and 17.5 for (c). Propagation distance $z$ is 1 for ($a_2$) and 6 for ($b_2$), ($c_2$).

$$I(t,\delta) = \ln\left|\int_{-\infty}^{+\infty} dt' A_{ref}(t'-t)A(t')e^{-i\delta t'}\right|. \quad (13)$$

Here $A_{ref}$ is an envelope of the reference pulse and $A$ is the envelope of the field inside the fiber. Let us assume that the reference pulse is a rectangular one with duration $\tau_{ref}$. Then knowledge of $I(\delta)$ for some fixed value of the delay $t$ gives us the spectrum of the part of the field selected by the values of $t$ and $\tau_{ref}$. The most common practical choice for the reference pulse is the pump pulse itself. Note that in order to calculate $I$, we use field envelopes, not the fields themselves. This leads to a certain frequency shift of our spectrograms with respect to the experimental ones.

To verify predictions for the resonance frequencies obtained by numerical solution of Eqs. (4) and (11) we carried out an extensive series of numerical experiments by modeling Eq. (1) with initial conditions

$$A(t,z=0) = a\sqrt{2q}\,\mathrm{sech}(t\sqrt{2q})e^{-i\delta_s t} + we^{-i\delta_{cw}t}. \quad (14)$$

Here $a$ and $w$ determine the amplitudes and $\delta_{s,cw}$ the frequencies of the pump pulse and cw. Modeling results for $\epsilon<0$ and $\epsilon>0$ shown in Figs. 1 and 2, respectively, demonstrate that our analytical predictions for the location of the resonance frequencies agree with numerics.

Regions of depletion of the cw pump in the spectrograms in Figs. 1 ($b_2$) and 2 ($b_2$), 2 ($c_2$) indicate that the large part of the energy transferred to the waves generated via FWM is taken from the cw pump and the soliton serves as a mediator in this transfer. If depletion of the cw pump is weak, as in Figs. 1($a_2$) and 2($a_2$), then the generated FWM signal is also weak. The length and direction of growth of the radiation tails and of the depletion regions are determined by the values and signs of the group velocities at the corresponding frequencies, which can be inferred from the slope of the $D(\delta)$ curve. For example, looking at Figs. 1($b_{1,2}$) one can see that the slope of $D(\delta)$ is negative for the frequencies corresponding to the Cherenkov radiation and to the cw pump (see points 5 and 1) and it is positive for the frequency corresponding to the FWM peak marked with 2. According to this, the tail of the Cherenkov radiation and the depletion region of the cw pump are acquiring negative delays with respect to the soliton, while the tail of the FWM radiation extends towards positive delays. Note that the FWM resonances generally have very different excitation efficiencies and in our numerical experiments we practically never observed two or more of them simultaneously. The group velocities of the soliton and of the cw pump are the same in the case shown in Figs. 1($c_{1,2}$) and the depletion region of the cw pump is located just opposite to the soliton. We have also demonstrated (see Appendix B) that the soliton in this case creates an effective repulsive potential for the dispersive waves at the frequency of the cw pump, which explains formation of the quasibound soliton-hole pair; see Fig. 1($c_2$).

In the Cherenkov case, the resonance wave serves as a sink for the energy, which is extracted from all the soliton Fourier components in such a way that the soliton structure of the gradually decaying pulse is preserved during propagation [17]. The soliton is also sustained as a coherent entity in the process of generation of the FWM signal; see Fig. 3. Total energy and momentum in the system are shared and exchanged between all the Fourier components of the soliton, the cw pump, and all the newly generated waves. Therefore, the wave number matching conditions (11) cannot be associated with conservation of the total momentum as it can be done in the textbook case of FWM between cw's [31].

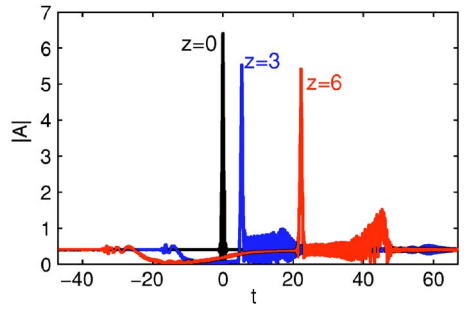


FIG. 3. (Color online) $|A|$ as a function of $t$ for $z=0,3,6$ obtained by solving Eq. (1) with the initial conditions (14). Parameters are $\epsilon=0.015$, $a=1$, $q=18$, $\delta_s=0$, $w=0.4$, and $\delta_{cw}=17.5$.

## V. AMPLITUDES OF THE GENERATED WAVES

In this section we develop an approach allowing us to estimate analytically the amplitudes of the emitted resonance waves. In order to achieve good agreement of the analytical and numerical results we need to abandon an assumption used in Sec. III that the cw pump is not affected by the FWM process. As our first step we assume that all the generated waves and cw pump are well separated spectrally and write

$$g = \psi_{ch}(z,t)e^{izD_{ch}-it\delta_{ch}} + \sum_{n=1}^{N}\psi_n(z,t)e^{izD_n-it\delta_n},$$

$$D_n = D(\delta_n), \quad D_{ch} = D(\delta_{ch}). \quad (15)$$

The first term in Eq. (15) is responsible for the Cherenkov resonance and the sum takes account of all the other resonances including the cw pump. We substitute Eq. (15) into Eq. (5) and assume that all $\psi_n$ are the slow functions of $t$ and $z$, so that we can neglect by the derivatives of $\psi_n$, which are higher than first, and by the nonlinear terms, which are not wave number matched.

Here we consider the case when Eqs. (9) and (10) have four real roots—i.e., $N=4$; see Figs. 1($b_1$,$c_1$) and 2($b_1$,$c_1$). The theory for the cases $N=2$ and $N=3$ is outlined in Appendix B. The structure of Eqs. (9) and (10), in the case of the cubic dispersion (4), is such that if one of them has three real roots, then the other one has only one. We assume that the resonance frequency originating from the single-root equation and the corresponding amplitude are numbered with $n=4$; see Fig. 1($b_1$). Then the resulting set of equations is

$$\partial_z\psi_n + D_n'\partial_t\psi_n - i2F^2\psi_n = iK_n, \quad n=1,2,3,4,$$

$$K_1 = F^2\{2\psi_2 e^{it[\delta_1-\delta_2]} + 2\psi_3 e^{it[\delta_1-\delta_3]} + \psi_4^* e^{it[\delta_1+\delta_4]}\},$$

$$K_2 = F^2\{2\psi_1 e^{it[\delta_2-\delta_1]} + 2\psi_3 e^{it[\delta_2-\delta_3]} + \psi_4^* e^{it[\delta_2+\delta_4]}\},$$

$$K_3 = F^2\{2\psi_1 e^{it[\delta_3-\delta_1]} + 2\psi_2 e^{it[\delta_3-\delta_2]} + \psi_4^* e^{it[\delta_3+\delta_4]}\},$$

$$K_4 = F^2\{\psi_1^* e^{it[\delta_4+\delta_1]} + \psi_2^* e^{it[\delta_4+\delta_2]} + \psi_3^* e^{it[\delta_4+\delta_3]}\}, \quad (16)$$

$$\partial_z\psi_{ch} + D'_{ch}\partial_t\psi_{ch} - i2F^2\psi_{ch} = ie^{it\delta_{ch}}\left[D(i\partial_t) - \frac{1}{2}\partial_t^2\right]F, \quad (17)$$

$$D'_n = \partial_\delta D(\delta_n), \quad D'_{ch} = \partial_\delta D(\delta_{ch}).$$

The equation for the Cherenkov field splits from the other equations. The solution of Eq. (17) has been studied in detail in [17] and will not be discussed here. The equation for $\psi_4$ is resonantly coupled to the equations for $\psi_{1,2,3}$ via the $F^2g^*e^{2iqz}$ term in Eq. (5). The fields corresponding to $\psi_{1,2,3}$ have the same wave numbers. Therefore, the corresponding equations are coupled via the $F^2g$ term in Eq. (5).

The results of our numerical modeling [see Fig. 1($b_2$)] indicate that the strongly dominant FWM process in this case happens when the cw pump and the resonance field both have their frequencies located between the soliton frequency, $\delta=0$, and the Cherenkov frequency, $\delta=\delta_{ch}$. Neglecting by the fields $\psi_{3,4}$, which are either not observed at all or negligibly small, we reduce Eqs. (16) to

$$\partial_z\psi_1 + D'_1\partial_t\psi_1 - i2F^2\psi_1 = i2F^2\psi_2 e^{it[\delta_1-\delta_2]}, \quad (18)$$

$$\partial_z\psi_2 + D'_2\partial_t\psi_2 - i2F^2\psi_2 = i2F^2\psi_1 e^{it[\delta_2-\delta_1]}. \quad (19)$$

To solve these equations it is useful to know the general solution to

$$\partial_z\psi_n + D'_n\partial_t\psi_n - i2F^2\psi_n = iK_n(t), \quad (20)$$

which is given by

$$\psi_n = \frac{ie^{iS_n(t)}}{D'_n}\left[B_n(t - D'_n z) + \int_{-\infty}^{t} dt' K_n(t')e^{-iS_n(t')}\right], \quad (21)$$

where $S_n=[2\sqrt{2q}\tanh(t\sqrt{2q})]/D'_n$ and $B_n$ is an arbitrary function of its argument. The initial condition $\psi_n(z=0)=0$ should be applied for the generated signal fields, and it is satisfied for

$$B_n = -\int_{-\infty}^{t-D'_n z} dt' K_n(t')e^{-iS_n(t')}. \quad (22)$$

The condition $\psi_n(z=0)=w$ should be used for the cw pump, and it is satisfied for

$$B_n = -iD'_n w - \int_{-\infty}^{t-D'_n z} dt' K_n(t')e^{-iS_n(t')}. \quad (23)$$

Let $\psi_1$ be the cw pump and $\psi_2$ be the generated signal. Using Eqs. (21)–(23) we can transform the differential equations (18) and (19) into a set of the integral equations

$$\psi_1 = we^{iS_1} + \frac{i2e^{iS_1}}{D'_1}\int_{t-zD'_1}^{t} dt' F^2\psi_2 e^{it'[\delta_1-\delta_2]-iS_1}, \quad (24)$$

$$\psi_2 = \frac{i2e^{iS_2}}{D'_2}\int_{t-zD'_2}^{t} dt' F^2\psi_1 e^{it'[\delta_2-\delta_1]-iS_2}. \quad (25)$$

Assuming that the potential created by the soliton and cw depletion is sufficiently weak, we can approximate the pump wave with $\psi_1 \approx we^{iS_1}$ and solve Eqs. (24) and (25) by iterations. Note that the phase of the cw component rotates on the soliton and changes its sign as $t$ varies from $-\infty$ to $+\infty$. The leading approximation for $\psi_2$ is then

$$\psi_2 \approx \frac{i2we^{iS_2}}{D'_2}\int_{t-zD'_2}^{t} dt' F^2 e^{it'[\delta_2-\delta_1]-iS_2+iS_1}. \quad (26)$$

The integral in Eq. (26) cannot be calculated exactly, but its value can be found in the limit of the large $z$ and $|t|$. Remembering that $z$ is always positive and assuming that $|D'_2 z/t|>1$ we find that if $D'_2<0$, then

$$\lim_{z\to\infty,t\to-\infty}\psi_2 = \frac{2we^{iS_2(-\infty)}\mathcal{J}}{iD'_2}, \quad \lim_{z\to\infty,t\to\infty}\psi_2 = 0, \quad (27)$$

and if $D'_2>0$, then

$$\lim_{z\to\infty,t\to-\infty}\psi_2 = 0, \quad \lim_{z\to\infty,t\to\infty}\psi_2 = \frac{2iwe^{iS_2(\infty)}\mathcal{J}}{D'_2}, \quad (28)$$

where

$$S_n(\pm\infty) = \pm 2\sqrt{2q}/D'_n, \quad (29)$$

$$\mathcal{J} = \int_{-\infty}^{\infty} dt F^2(t)e^{it[\delta_2-\delta_1]-iS_2(t)+iS_1(t)}. \quad (30)$$

The integral (30) can be calculated either numerically or in an approximate analytical form. Using the fact that $F^2$ is localized around zero, we can replace the function $S_n(t)$ by its linear approximation valid for $t$ close to zero: $S_n(t) \approx 4qt/D'_n$. Then,

$$\mathcal{J} \approx \int_{-\infty}^{\infty} dt F^2 e^{it4\Omega_-} = \frac{2\pi\Omega_-}{\sinh(\pi\Omega_-/\sqrt{2q})\cosh(\pi\Omega_-/\sqrt{2q})}, \quad (31)$$

$$\Omega_- = \frac{\delta_2-\delta_1}{4} - q\frac{D'_1-D'_2}{D'_1D'_2}. \quad (32)$$

Numerically solving Eq. (1) and taking the Fourier transform of $A$ we can calculate the rate $\Gamma$ of the energy change at a particular frequency. An approximate analytical expression for this rate at the frequency of the FWM signal is given by $\Gamma \approx d/dz$[length of the radiation tail $\times$ (tail amplitude)$^2$] $\approx 4w^2\mathcal{J}^2/D'_2$. Figure 4 shows $\Gamma$ as the function of the cw frequency. One can see that the explicit analytical expression (31) (see the dashed line) gives reasonable agreement with numerical calculations of the integral in Eq. (30) (see the solid line). Comparison of the results for $\Gamma$ obtained from the direct numerical modeling of Eq. (1) and from Eqs. (30) and (31) is good only when depletion of the cw pump is small and the iterative method of solving Eqs. (24) and (25) is applicable. This condition is satisfied outside the regions of

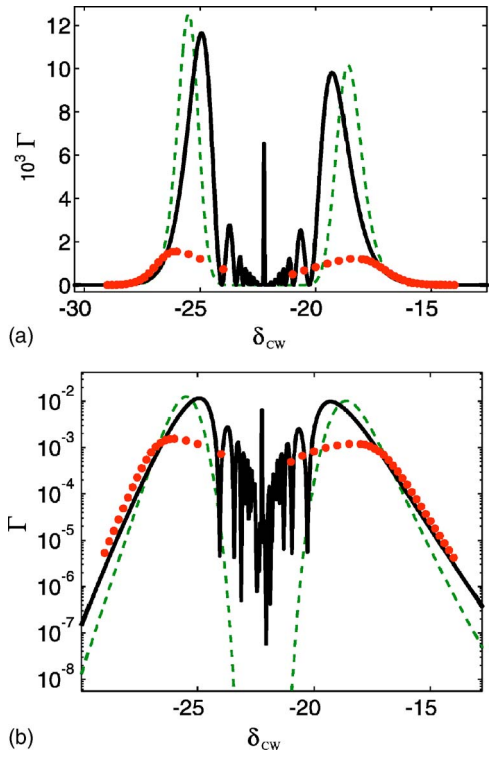


FIG. 4. (Color online) (a) The rate $\Gamma$ of the energy change at the frequency of the FWM signal as a function of the frequency of the cw pump, $\delta_{cw}$. The dashed line is obtained using an analytical approximation for $\mathcal{J}$; see Eq. (31). The solid line corresponds to the numerical calculation of $\mathcal{J}$ using Eq. (30), and the dots are obtained from the numerical solution of Eq. (1). Parameters are $\epsilon=-0.015$, $a=1$, $q=3$, $\delta_s=0$, and $w=0.02$. (b) is the same as (a) but plotted in the logarithmic scale.

the two maxima of $\Gamma(\delta_{cw})$ [see Figs. 4(a) and 4(b)]; here, $\delta_{cw}=\delta_1$. We should notice, however, that some discrepancy [see dotted and full lines in Fig. 4(b)] is preserved even when the depletion of the pump is negligible. This is attributed to the shift of the soliton central frequency due to the spectral recoil effect, which has not been taken into account so far; see more detailed discussion in Sec. VII.

Let us now summarize and discuss the above results. Equations (18) and (19) describe the interaction of the two waves within and by means of the potential created by the soliton. The pump wave stimulates the signal wave to escape from the potential. The reduction of the problem to the integral equations (24) and (25) and the iterative method of their solution are similar to the integral equations of the classical and quantum scattering theories and to the Born method [32]. In the Born approach the amplitude of the scattered field in the far zone of the potential is proportional to the amplitude of a Fourier component of the potential [32]. This relates to the fact that in the leading order of the Born theory the potential is simply disregarded. Similarly, we could disregard the soliton potential on the left-hand sides of Eqs. (18) and (19); then, the $q$ term in Eq. (32) would disappear. This term originates from the rotation of the phases of the signal and pump waves (see $S_{1,2}$ functions) introduced by the soliton potential. The phase rotation is important because the

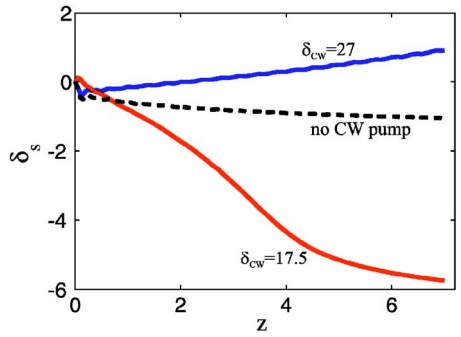


FIG. 5. (Color online) Change of the soliton frequency $\delta_s$ with propagation due to the spectral recoil effect, as calculated from Eq. (1) with $\epsilon=0.015$. Initial parameters for the $\delta_{cw}=27$ case are the same as for Fig. 2(b) and for the $\delta_{cw}=17.5$ case are the same as for Fig. 2(c). The dashed line demonstrates the spectral recoil effect due to Cherenkov radiation only—i.e., in the absence of the cw pump.

spectral amplitude of the exponentially localized potential is exponentially sensitive to the value of the frequency at which it is calculated. The influence of this effect on the theoretical predictions of the amplitude of the Cherenkov radiation has been analyzed in detail in our previous work [17].

## VI. DEPLETION OF THE CW PUMP

The depletion of the field at the frequency of the cw pump can be described only in the second order of our iterative procedure, which does not make the strongest case for a good comparison between numerical and analytical results. However, the mere fact of the existence of the depletion can be derived from the relatively simple calculations. Substituting Eq. (26) into Eq. (24) we find that the amplitude of the cw pump is given by

$$\psi_1 \approx we^{iS_1(t)} - \frac{4we^{iS_1(t)}}{D_1'D_2'}\int_{t-zD_1'}^{t} dt' F^2(t')e^{it'[\delta_1-\delta_2]-iS_1(t')+iS_2(t')} \times \int_{t'-zD_2'}^{t'} dt'' F^2(t'')e^{it''[\delta_2-\delta_1]-iS_2(t'')+iS_1(t'')}. \quad (33)$$

Using the same arguments as before we can replace the limits of the integrals in Eq. (33) with $\pm\infty$ and find that $|\psi_1| \approx |w|\{1+4\mathcal{J}^2/[D_1'D_2']\}$. $D_1'D_2'<0$ [see points 1 and 2 in Fig. 1(b$_1$)], and hence the above result predicts depletion of the cw pump.

## VII. SPECTRAL RECOIL

The drift of the carrier frequency of the soliton $\delta_s$ induced by the FWM has been already mentioned above, and it is explicitly demonstrated in Fig. 5. In the absence of the Raman effect this drift is solely attributed to the spectral recoil effect originating from the interaction of the dispersive waves with the soliton. We assume that the total field momentum $M=1/[2i]\int dt[A^*\partial_t A - A\partial_t A^*]$ can be approximately divided into the soliton momentum and momenta of all the dispersive waves. Conservation of $M$—i.e., $\partial_z M=0$—implies that the changes of the momenta of the participating disper-

sive waves must be compensated for by the change of the soliton momentum. This gives us the balance equation

$$Q_s \partial_z \delta_s = -\delta_{ch} D'_{ch} |\psi_{ch}|^2 - \{\delta_2 D'_2 |\psi_2|^2 + \delta_1 D'_1 [|\psi_1|^2 - w^2]\}. \quad (34)$$

Here $Q_s = \int dt |F|^2$ is the soliton energy and $\partial_z \delta_s$ is the change of the soliton frequency with $z$ [17]. The subscripts 1 and 2 mark the quantities related to the cw pump and FWM signal, respectively. $|\psi_1|^2 - w^2 < 0$ is the difference in the amplitudes of the depleted and initial cw pump. The graph with $\delta_{cw} = 27$ in Fig. 5 corresponds to Figs. $2(b_{1,2})$ and the graph with $\delta_{cw} = 17.5$ to the Figs. $(c_{1,2})$.

The term $\delta_{ch} D'_{ch} |\psi_{ch}|^2$ is positive in the both cases, and therefore the Cherenkov effect tends to decrease the soliton frequency—i.e., leads to the red recoil. The recoil originating from the Cherenkov radiation only has been analyzed in detail in Ref. [17]. The expression inside $\{\}$ characterizes influence of the FWM on the change in the soliton frequency. It can be seen that the both terms inside $\{\}$ have the same sign for the cases shown in Figs. 2(b) and 2(c). Namely, $\{\}$ is negative—i.e., FWM leads to the blue recoil—in the case of Figs. $2(b_{1,2})$ and it is positive—i.e., FWM leads to the red recoil—in the case of Figs. $2(c_{1,2})$. The dashed line in Fig. 5 shows the relative smallness of the recoil originating from the Cherenkov radiation only—i.e., $w = 0$. One can see that the recoil from the FWM process is much stronger, and it determines overall direction in the drift of the soliton frequency, in agreement with the above predictions derived from the balance equation (34).

## VIII. ROLE OF THE FOUR-WAVE MIXING RESONANCES IN SUPERCONTINUUM GENERATION

In experiments on supercontinuum the fiber is pumped with pulses only. Under sufficiently common conditions a single pump pulse generates both solitons and dispersive waves, which mix and interact within the fiber. The interpretation of many experimental measurements is still causing certain controversy. Therefore, we found it instructive to summarize the main features of supercontinuum spectra, the origin of which lies in the FWM between solitons and dispersive waves and which can be understood using the theory developed above. The Raman effect is important in the experiments with femtosecond pulses therefore in this section of the paper we add the Raman term $iA\int_{-\infty}^{+\infty} R(t') |A(t - t', z)|^2 dt'$ to the right-hand side of Eq. (1). Here $R(t)$, is the Raman response function of silica; see Appendix A.

### A. Pump at the zero GVD wavelength: FWM of solitons and relict radiation

To achieve efficient generation of supercontinuum the pump frequency is often selected to coincide with the zero GVD frequency: $\partial_\delta^2 D(\delta) = 0$. At the first stage of the evolution the pulse breaks up into two spectral parts located on the opposite sides from the zero GVD point; see Fig. 6 and [1,10,24–26]. These parts are approximately equally detuned from the zero GVD point and therefore propagate with close group velocities. The part located in the anomalous GVD region forms a soliton or a few, while the part in the normal GVD region is formed from the dispersive waves only, and it will be called *relict radiation*. The parabolic shape of the XFROG spectrograms in Figs. $6(a_{1,2})$ and $6(b_{1,2})$ is due to the parabolic shape of $\partial_\delta D(\delta)$. The up or down orientation of the parabolas is determined by the sign of $\epsilon$. The soliton emerging in the anomalous GVD region efficiently interacts with the part of the relict radiation propagating with the same group velocity. Therefore we naturally expect that the result of this interaction should be similar to the case presented in Figs. $1(c_{1,2})$. Indeed, in Figs. $6(a_1)$ and $6(b_1)$ one can see the formation of the depletion region in the relict radiation directly opposite to the soliton.

With further propagation distance the XFROG spectrograms for the cases $\epsilon > 0$ and $\epsilon < 0$ become qualitatively distinct. In particular, in the case $\epsilon > 0$ the new spectral lines emerge outside the right branch of the parabola [see Fig. 6 $(a_2)$ and Refs. [10,25,26]], causing further spectral broadening. In the case $\epsilon < 0$ the new spectral lines are formed between the two branches of the parabola; see Fig. $6(b_2)$ and Ref. [24]. One can clearly see that in the both cases new spectral lines are starting to form in the regions of the time domain adjacent to the solitons. We argue below that the new spectral features are the FWM resonances between the solitons and relict radiation.

Raman effect plays a key role in understanding of these new peaks. Indeed, as propagation distance increases the Raman induced soliton self-frequency shift towards the red part of the spectrum becomes noticeable [31]. This destroys the synchronism of the group velocities between the soliton and the depleted part of the relict radiation, thereby removing degeneracy of the FWM resonance and cw pump; compare, e.g., Figs. 1(c) and 1(b). In the case $\epsilon > 0$ [see Fig. $6(a_{1,2})$], the corresponding wave number matching diagram becomes qualitatively similar to Fig. $2(c_1)$ and in the case $\epsilon < 0$ [see Fig. $6(b_{1,2})$] to Fig. $1(b_1)$. This explains location of the new spectral peaks. Note that if the fiber is pumped at or close to the zero GVD wavelength, then the Cherenkov radiation usually appears after the FWM peaks are generated.

### B. Pump in the anomalous GVD region: FWM of solitons and Cherenkov radiation

If the pump wavelength is in the anomalous GVD region and $\epsilon < 0$, then the redshifted Cherenkov radiation is strongly amplified through the mechanism described in details in Refs. [16,17]. Furthermore, if the pump pulse is sufficiently strong to give birth to more than one soliton, then the second and subsequent solitons are always born inside the tail of the Cherenkov radiation emitted by the strongest primary soliton; see Figs. $6(c_{1,2})$. Mixing of the Cherenkov radiation with the secondary solitons results in the generation of the FWM peaks; see Figs. $6(c_{1,2})$. The wave number matching diagram qualitatively corresponding to this case is shown in Fig. $1(b_1)$. Experimental measurements of this effect have been published in Ref. [24].

## IX. SUMMARY

We have presented a thorough theoretical and numerical investigation of the generation of new frequencies resulting

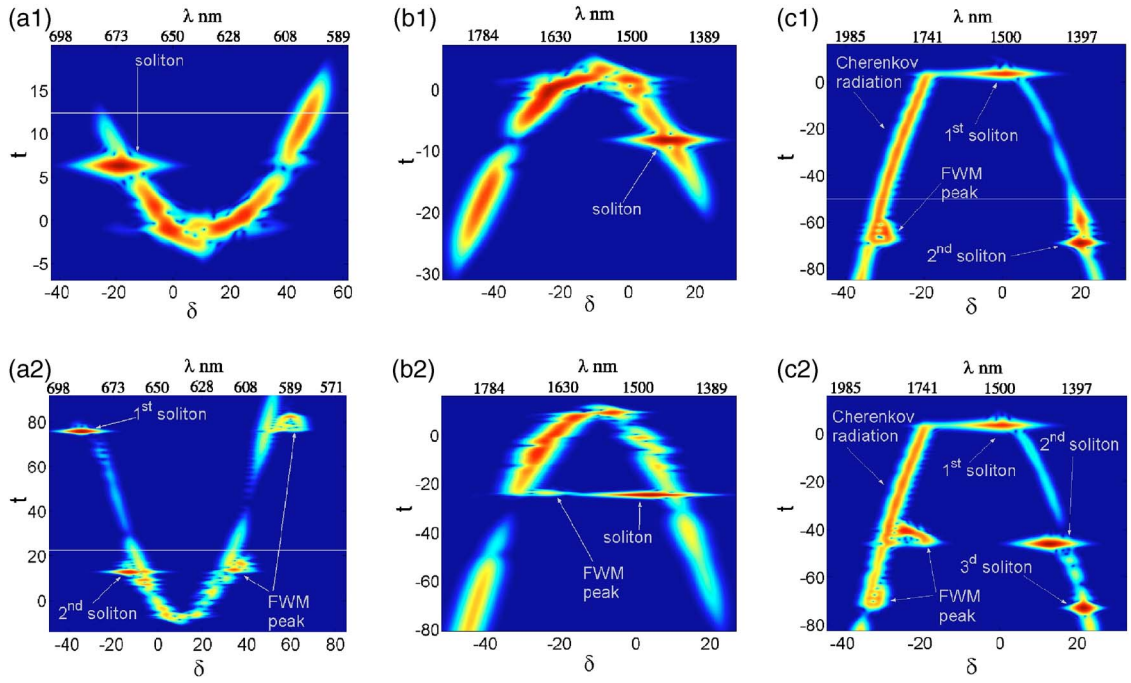


FIG. 6. (Color online) Modeling of supercontinuum generation in a fiber with $\gamma=0.05/[\mathrm{Wm}]$ pumped with femtosecond optical pulses. ($a_{1,2}$) Pump wavelength coincides with the zero GVD wavelength at 638 nm, GVD slope $\partial_\omega\beta_2=0.9$ ps$^3$/km, $\tau=200$ fs, peak pump power 3.6 kW, and propagation distances are 0.24 m ($a_1$) and 1.12 m ($a_2$). Corresponding dimensionless parameters are $a=4.6$, $q=3.4$, $\epsilon=0.015$, $\delta_s=11$, $z_1=0.3$, and $z_2=1.4$. ($b_{1,2}$) Pump wavelength coincides with the zero GVD wavelength at 1570 nm, GVD slope $\partial_\omega\beta_2=-0.9$ ps$^3$/km, $\tau=200$ fs, peak pump power 3.6 kW, and propagation distances are 0.4 m ($a_1$) and 1.44 m ($a_2$). Corresponding dimensionless parameter are $a=4.6$, $q=3.4$, $\epsilon=-0.015$, $\delta_s=-11$, $z_1=0.5$, and $z_2=1.8$. ($c_{1,2}$) Pump wavelength is in the anomalous GVD region at 1432 nm, fiber has the zero GVD wavelength at 1651 nm, $\beta_2=-50$ ps$^2$/km, GVD slope $\partial_\omega\beta_2=-0.68$ ps$^3$/km, $\tau=150$ fs, peak pump power 3.6 kW ($c_1$) and 4.4 kW ($c_2$), and propagation distance 1.12 m. Corresponding dimensionless parameters are $a=3.47$ ($c_1$), $a=3.85$ ($c_2$), $\epsilon=-0.015$, $\delta_s=15$, and $z=2.5$.

from the mixing of solitons and dispersive waves in optical fibers with higher-order dispersions and demonstrated the importance of this process for understanding of the optical supercontinuum observed in photonic crystal fibers.

The wave number matching condition [see Eq. (12) for $J=\pm1$] determining frequencies of the newly generated waves is formally identical to the textbook wave number matching condition for the FWM of cw's; see, e.g., Chap. 10 in [31]. However, the physical interpretation of Eq. (12) has important differences from the standard case. In the case of FWM between the continuous dispersive waves, the two pump photons at the same or different frequencies $\omega_{p1}$ and $\omega_{p2}$ are transformed via virtual transitions into the two signal photons with frequencies $\omega_{s1}$ and $\omega_{s2}$. The photon energy is conserved during this process, so that $\omega_{p1}+\omega_{p2}=\omega_{s1}+\omega_{s2}$. In our case the input cw actually interacts with all Fourier components of the solitons. Therefore no energy conservation law involving only four frequencies associated with the four wave numbers involved in the matching condition exists in our case. Momentum conservation also can be applied only for all Fourier harmonics of the soliton plus the input and generated cw's; see Eq. (34).

To find the signal emerging from the scattering of the cw pump on the soliton we reduce the problem to a system of integral equations, which are then solved by iterations. In this way we have been able to calculate the amplitudes of the generated waves and predict depletion of the cw pump. Using conservation of the total momentum we have predicted a shift of the soliton carrier frequency due to spectral recoil from the input and generated cw's.

## ACKNOWLEDGMENTS

The authors acknowledge discussions with F. Biancalana, A. Efimov, I. Gabitov, J. Knight, and P. Russell. This work is supported by the Leverhulme Trust.

## APPENDIX A

Here we discuss normalization of the variables and parameters in Eq. (1). The variable $t$ is the time in the reference frame moving with the group velocity $v_0=v(\omega_0)$ and measured in the units of $\tau$: $t=[T-z/v_0]/\tau$, where $T$ is the physical time, $\tau$ is the normalization constant close to the pulse duration, and $\omega_0$ is the reference frequency. $\delta$ is the normalized detuning of the physical frequency $\omega$ from $\omega_0$—i.e., $\omega-\omega_0=\delta/\tau$. If $\beta(\omega)$ is the frequency dependence of the propagation constant of the fundamental fiber mode, then

$$D(\delta)=\{\beta(\omega_0+\delta/\tau)-\beta(\omega_0)-\beta_1(\omega_0)\delta/\tau\}L_{gvd}, \quad \text{(A1)}$$

where $\beta_n(\omega)=\partial_\omega^n\beta(\omega)$ and $L_{gvd}=\tau^2/|\beta_2(\omega_0)|$ is the GVD length. Thus the Fourier image of the operator $D(i\partial_t)$ is, in fact, the properly shifted and normalized propagation constant of the fiber mode. $z=Z/L_{gvd}$, where $Z$ is the distance

along the fiber. The field amplitude in Eq. (1) is measured in units of $\sqrt{P_0}$, where $P_0=1/[\gamma L_{gvd}]$ is the peak power of the fundamental soliton with duration $\tau$—i.e., $q=1/2$—and $\gamma$ is the nonlinear fiber parameter [31]. Link of $\epsilon$ in Eq. (4) with the real-world parameters is given by $\epsilon=\partial_\omega\beta_2(\omega_0)/[6\tau|\beta_2(\omega_0)|]$, and its sign is determined by the slope of $\beta_2(\omega)$. The Raman response function introduced in Sec. VIII is given by $R(t)=[1-\theta]\Delta(t)+\theta[\tau_1^2+\tau_2^2]\Theta(t)/[\tau_1\tau_2^2]$, where $\Delta(t)$ is the Dirac delta function, $\Theta(t)$ is the Heaviside function, $\theta=0.18$, $\tau_1=12.2$ fs/$\tau$, and $\tau_2=32$ fs/$\tau$ [31].

## APPENDIX B

In the case, when there are only two FWM resonances, $N=2$ [see Figs. 1($a_{1,2}$) and 2($a_{1,2}$)], the resulting set of equations for the slowly varying amplitudes is

$$\partial_z\psi_1+D_1'\partial_t\psi_1-i2F^2\psi_1=iF^2\psi_2^*e^{it[\delta_1+\delta_2]}, \tag{B1}$$

$$\partial_z\psi_2+D_2'\partial_t\psi_2-i2F^2\psi_2=iF^2\psi_1^*e^{it[\delta_1+\delta_2]}. \tag{B2}$$

Here numbering of the $\psi_n$ functions corresponds to the numbering of the resonant frequencies in Fig. 1($a_1$). Equations for $\psi_{1,2}$ couple via $F^2g^*e^{i2qz}$ in Eq. (5). Solutions to Eqs. (B1) and (B2) are found in the same way, as was done for Eqs. (18) and (19). Assuming that $\psi_1$ is the cw pump and $\psi_2$ is the generated signal we find

$$\psi_2\approx\frac{iwe^{iS_2}}{D_2'}\int_{t-zD_2'}^{t}dt'F^2e^{it'[\delta_1+\delta_2]-iS_2-iS_1}. \tag{B3}$$

Then Eqs. (27) and (28) can be used with

$$\mathcal{J}=\int_{-\infty}^{\infty}dtF^2(t)e^{it[\delta_1+\delta_2]-iS_2(t)-iS_1(t)}$$

$$\approx\frac{2\pi\Omega_+}{\sinh(\pi\Omega_+/\sqrt{2q})\cosh(\pi\Omega_+/\sqrt{2q})},$$

$$\Omega_+=\frac{\delta_2+\delta_1}{4}-q\frac{D_1'+D_2'}{D_1'D_2'}. \tag{B4}$$

The next-order approximation for the amplitude of the field at the cw-pump frequency is $|\psi_1|\approx|w|\{1-4\mathcal{J}^2/[D_1'D_2']\}$, where $D_1'D_2'>0$.

In the case $N=3$ the two resonance frequencies are degenerate and the group velocity of the soliton coincides with the group velocity corresponding to the degenerate resonance, where $D'=0$; see Fig. 1($c_1$). Therefore for the degenerate point the second-order dispersion becomes a dominant term and must be accounted for when we use the ansatz (15) and slowly varying approximation. If the cw-pump frequency coincides with the point of degeneracy, point 1 in Fig. 1($c_1$), then strong changes happen to the pump itself, while the other two waves, points 2 and 3, can be disregarded. The governing equation for the $\psi_1$ amplitude is then

$$i\partial_z\psi_1=\frac{D_1''}{2}\partial_t^2\psi_1-2F^2\psi_1. \tag{B5}$$

Equation (B5) is a Schrödinger equation with $D_1''>0$. This equation describes excitations with the negative effective mass, which are repelled by the potential well created by the soliton. This explains formation of the depletion region in the pump field opposite to the soliton in the XFROG spectrograms shown in Figs. 1($c_2$) and 6($a_1$,$b_1$).


[1] P. K. A. Wai, C. R. Menyuk, H. H. Chen, and Y. C. Lee, Opt. Lett. **12**, 628 (1987).
[2] P. Beaud, W. Hodel, B. Zysset, and H. P. Weber, IEEE J. Quantum Electron. **23**, 1938 (1987).
[3] M. N. Islam, G. Sucha, I. Bar-Joseph, M. Wegener, J. P. Gordon, and D. S. Chemla, J. Opt. Soc. Am. A **6**, 1149 (1989).
[4] P. Dumais, F. Gonthier, S. Lacroix, J. Bures, A. Villeneuve, P. G. J. Wigley, and G. I. Stegeman, Opt. Lett. **18**, 1996 (1993).
[5] T. A. Birks, W. J. Wadsworth, and P. St. J. Russell, Opt. Lett. **25**, 1415 (2000).
[6] J. K. Ranka, R. S. Windeler, and A. J. Stentz, Opt. Lett. **25**, 25 (2000).
[7] A. L. Gaeta, Opt. Lett. **27**, 924 (2002).
[8] A. Ortigosa-Blanch A, J. C. Knight, and P. S. J. Russell, J. Opt. Soc. Am. B **19**, 2567 (2002).
[9] S. G. Leon-Saval, T. A. Birks, W. J. Wadsworth, P. St. J. Russell, and M. W. Mason, Opt. Express **12**, 2864 (2002).
[10] J. M. Dudley, X. Gu, L. Xu, M. Kimmel, E. Zeek, P. O'Shea, R. Trebino, S. Coen, and R. S. Windeler, Opt. Express **10**, 1215 (2002).
[11] J. Herrmann, U. Griebner, N. Zhavoronkov, A. Husakou, D. Nickel, J. C. Knight, W. J. Wadsworth, P. St. J. Russell, and G. Korn, Phys. Rev. Lett. **88**, 173901 (2002).
[12] W. H. Reeves, D. V. Skryabin, F. Biancalana, J. C. Knight, P. St. J. Russell, F. G. Omenetto, A. Efimov, and A. J. Taylor, Nature (London) **424**, 511 (2003).
[13] G. Genty, M. Lehtonen, H. Ludvigsen, J. Broeng, and M. Kaivola, Opt. Express **10**, 1083 (2002).
[14] G. Genty, M. Lehtonen, H. Ludvigsen, and M. Kaivola, Opt. Express **12**, 3471 (2004).
[15] I. Cristiani, R. Tediosi, L. Tartara, and V. Degiorgio, Opt. Express **12**, 124 (2004).
[16] D. V. Skryabin, F. Luan, J. C. Knight, and P. St. J. Russell, Science **301**, 1705 (2003).
[17] F. Biancalana, D. V. Skryabin, and A. V. Yulin, Phys. Rev. E **70**, 016615 (2004).
[18] P. K. A. Wai, H. H. Chen, and Y. C. Lee, Phys. Rev. A **41**, 426 (1990).
[19] V. I. Karpman, Phys. Rev. E **47**, 2073 (1993).
[20] V. I. Karpman, Phys. Rev. E **62**, 5678 (2000).
[21] V. I. Karpman, Phys. Scr. **T82**, 44 (1999).
[22] N. Akhmediev and M. Karlsson, Phys. Rev. A **51**, 2602

(1995).
[23] A. V. Yulin, D. V. Skryabin, and P. St. J. Russell, Opt. Lett. **24**, 2411 (2004).
[24] A. Efimov, A. J. Taylor, F. G. Omenetto, A. V. Yulin, N. Y. Joly, F. Biancalana, D. V. Skryabin, J. C. Knight, and P. St. J. Russell, Opt. Express **12**, 6498 (2004).
[25] G. Genty, M. Lehtonen, and H. Ludvigsen, Opt. Express **12**, 4614 (2004).
[26] T. Hori, N. Nishizawa, T. Goto, and M. Yoshida, J. Opt. Soc. Am. B **21**, 1969 (2004).
[27] N. Akhmediev and S. Wabnitz, J. Opt. Soc. Am. B **9**, 236 (1992).
[28] E. A. Kuznetsov, A. V. Mikhailov, and I. A. Shimokhin, Physica D **87**, 201 (1995).
[29] Q. H. Park and H. J. Shin, Phys. Rev. Lett. **82**, 4432 (1999).
[30] H. J. Shin, Phys. Rev. E **67**, 017602 (2003).
[31] G. P. Agrawal, *Nonlinear Fiber Optics* (Academic Press, San Diego, 2001).
[32] M. Born and E. Wolf, *Principles of Optics* (Cambridge University Press, Cambridge, England, 2002).